IEEE Access
Multidisciplinary | Rapid Review | Open Access Journal

Received October 24, 2019, accepted November 12, 2019, date of publication November 25, 2019,
date of current version December 11, 2019.

Digital Object Identifier 10.1109/ACCESS.2019.2955556

State Estimation Approach of Lithium-Ion Batteries by Simplified Ultrasonic Time-of-Flight Measurement

HARTMUT POPP[1,2], (Student Member, IEEE), MARKUS KOLLER[1], SEVERIN KELLER[2], GREGOR GLANZ[1], REINHARD KLAMBAUER[2], AND ALEXANDER BERGMANN[2]
[1]Center for Low-Emission Transport, AIT Austrian Institute of Technology, 1210 Vienna, Austria
[2]Institute of Electronic Sensor Systems, Graz University of Technology, 8010 Graz, Austria

Corresponding author: Hartmut Popp (hartmut.popp@ait.ac.at)

This work was supported by the Austrian Research Promotion Agency (FFG) under Grant 865148.

ABSTRACT This work presents an approach to monitoring the State-Of-Charge of Lithium-Ion battery cells via piezo disc-based ultrasonic Time-Of-Flight measurement by measuring the traveling time of a mechanical pulse through the cell between two surface-mounted sensors. The main advantage of this approach is the simplicity and the resulting low cost, which makes it suitable for future application in battery management systems. In detail, the excitation of the piezo actuator is done using a single semiconductor switch instead of a power amplifier, and the received signal is processed with an amplifier and Schmitt-trigger combination to condition the signal for the microprocessor, which is part of a battery management system. Both the functionality and the limits of the design are evaluated with a high energy density Lithium-Ion pouch cell under different operational scenarios. Several parameters such as temperature, current rates, and excitation frequency are varied to prove the design concept. For validation purposes, an estimation function is generated and a real-world driving cycle applied. An estimation with an error of 1.29 % of the Time-Of-Flight total value or 16.85 % of the State-Of-Charge value under challenging conditions is achieved with the current setup.

INDEX TERMS Battery management system, diagnostics, lithium-ion battery, piezoelectric transducers, state-of-charge, time-of-flight, ultrasonic.

I. INTRODUCTION

Due to their high energy density and long lifetime, Lithium-Ion batteries (LIBs) are nowadays predominant in mobile applications, modern stationary storage solutions, and in electric vehicles, and will maintain this position in the near and mid-term future [1]. One very important aspect of ensuring the longevity and safety of LIBs is proper operation within the constraints of the systems. This is the task of the battery management system (BMS). Determining the state-of-charge (SOC) of the battery is one of its key functionalities [2], [3]. Xiong et al. [3] in their review state that in principle there are four groups of methods to do so:

1) lookup table,
2) ampere-hour integral,
3) model based estimation, and
4) data driven.

These methods have in common that they all rely on measurement of the electrical two-pole behaviour of the cell, with the more sophisticated methods combining the actual measurement with cell temperature and operational history of the battery. So, the SOC is measured in an indirect way, or derived from other values.

In recent years, methods where the SOC is determined in a direct way via non-destructive, in-situ measurements of the properties of the active materials in the cell have been investigated more deeply by various research groups. The reason is that during operation the Li^+ ions move from anode to cathode upon discharge and vice versa during charge. This leads to SOC-dependent structural changes in both electrodes, with a very pronounced change for anodes containing e.g. graphite [4] or silicon [5]. While graphite expands up

The associate editor coordinating the review of this manuscript and approving it for publication was Fabio Massaro.

to around 10 % from the unlithiated to the lithiated state, the change becomes drastic for silicon, which can expand by around 300 %, so in the future direct determination will be of even higher relevance. There are three main groups of methods to determine the internals states:

1) imaging,
2) dilatometry, and
3) acoustics,

with the first and second having been employed on LIB full cells since the beginning of this century [6], [7] while the third has been receiving more attention over the last years [2], [8]–[12]. Hsieh *et al.* [8] employ acoustic ultrasonic measurements in transmission and reflection geometry, Ladpli *et al.* [9], [10] and Gold *et al.* [2] combine ultrasonic time-of-flight (TOF) and amplitude measurements, and Popp *et al.* [11] use acoustic signals in the audible range. All authors were able to identify correlations between the acoustic response of the system and the SOC, and partially also the SOH. All authors used complex and expensive lab equipment and did tests with artificial cycles that cannot be found in real world applications. Only one work [11] investigated the phenomena at different temperatures and found significant dependencies.

This work now opted for utilization of the technique of acoustic ultrasonic surface TOF signals in the range of 25 kHz to 40 kHz, as they are comparatively easy to measure. The whole setup aims at integration into a BMS. Thus, it is designed with electronic equipment of a total additional cost in the single-digit Euro range per unit, excluding economies of scale. To achieve the stated cost reduction, the circuit was assembled with inexpensive piezo actuator discs; instead of excitation with an amplifier and the corresponding complex signal generation, control of the actuator disc was maintained with an electronic switch, while the measurement of the TOF employing a Schmitt-trigger based circuit and the possibility to control the circuit using spare channels on the existing microprocessor from the BMS were realized.

The designed circuit passed the initial functionality tests. Feasibility tryouts and TOF behaviour were investigated on an off-the-shelf 12 Ah high energy pouch cell at different experimental conditions. The cell was operated with a real world driving cycle, the worldwide harmonized light vehicle test procedure (WLTP) [13] cycle. WLTP is the standard test nowadays for evaluation of energy consumption of passenger cars and reflects various realistic loads from everyday operation. The obtained results are discussed in terms of their accuracy, the limitations are evaluated, and the feasibility of application of the TOF approach for SOC estimation is evaluated.

II. TIME-OF-FLIGHT MEASUREMENT ON LIB

The TOF method is well known in other applications but requires adaptation to be usable for LIB state estimation. This section first provides the theoretical background on the mechanical composition and behaviour of LIB pouch cells regarding TOF measurement and then presents a practical approach to implementing the method in a BMS.

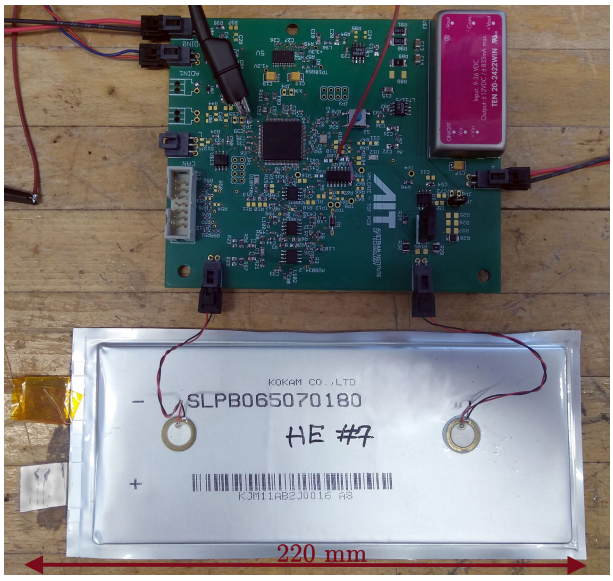

FIGURE 1. Developed PCB and cell connected to piezo transducer discs placed on pouch cell.

A. THEORETICAL BACKGROUND

During battery operation, the lithiation level of the anode, representative of SOC, has a significant impact on cell behaviour, ageing, and cyclability. Because of the complex physicochemical nature of the lithium-ion battery, identifying the internal changes that lead to battery degradation and failure is challenging, but as a feature of interest extracted from a non-destructive ultrasonic response signal, TOF could be used for analysing battery performance, which leads to changes in both mechanical impedance and ultrasonic velocity [9], [14], [15]. The lithium concentration affects the Young's modulus and the density of the graphite electrode [16]. This influences the ultrasonic wave propagation speed, the latter being indirectly dependent on the SOC. For example, a high lithium concentration in the electrode alters the Young's modulus and therefore causes a higher wave propagation velocity.

For the measurement an emitter and a receiver, in this case piezo discs, are placed on the cell under test at a known distance from each other (Fig. 1). The emitter sends an ultrasonic signal burst that propagates through the battery cell and is detected by the receiver. The time between emitting and receiving the signal is measured as TOF. The battery cell consists of thin layers of anode, cathode, separator and, current collector materials. As the thickness of these layers is smaller than the wavelength of the propagating waves, the waves are considered to behave as Lamb waves. Lamb waves are guided waves in thin plates and can propagate over long distances with little attenuation. Lamb waves are dispersive, enabling the determination of elastic properties and the thickness of the plate [17].

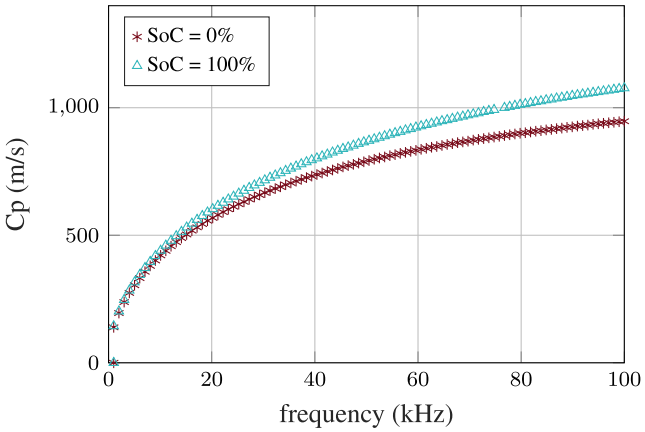

FIGURE 2. Calculated velocities of an empty and a fully charged LIB cell.

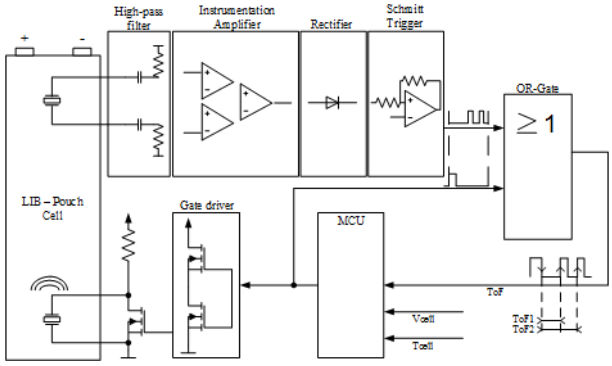

FIGURE 3. Functional diagram of TOF setup and implementation.

A calculation of the wave velocities for different frequencies can be found in Fig. 2. The formula for this calculation is in the appendix. It was found that frequencies above 20 kHz show significant differences between a fully charged and a fully discharged cell. The greater the difference in velocity, the greater the difference in TOF, permitting a less complex, or more accurate, measuring system. In addition, lower frequencies also have lower demands on excitation and measurement. Thus, frequencies in the region between 25 kHz and 40 kHz were chosen for this study. As the sensors were placed 10 cm from each other, the TOF of the signal at e.g. 25 kHz was expected to be between 161 μ s for a fully discharged and 150 μ s for a fully charged cell.

B. IMPLEMENTATION FOR A BMS

Ladpli *et al.* [9], [10] and Gold *et al.* [2] showed that changes in LIB can be detected both by the variation in the amplitude at the receiver and by the TOF through the cell. Because of a reduced sampling rate and less effort for signal processing, TOF measurement makes lower demands on the hardware than processing the variation in amplitude. As cost plays a major role in the field of battery applications [1] this work focuses on the implementation of a low-cost TOF approach that could be used in a BMS. Piezo transducers are utilized both as actuator and sensor. Both are commercial piezo discs from PUI Audio (Dayton, OH, USA) type AB1290B-LW100-R with a resonance frequency of 9 kHz and a capacitance of 8 nF. They are directly attached on the longitudinal axis of the cell, each 5 cm away from the centre and fixed in position with epoxy glue (Fig. 1).

Fig. 3 shows the block diagram of the ultrasonic sensing system. The main components are the two piezo discs, the microcontroller, the transmitter circuit, and the receiver circuit. The receiver circuit consists of a high pass filter with a cut-off frequency of 3.3 kHz. This filter reduces low frequency noise, which can occur from mechanical vibrations in the environment. The filtered signal is amplified by an instrumentation amplifier with a gain factor of 201. The rectifier, which consists of a simple single diode, cuts off the negative voltage of the amplified signal. The rectified signal is fed into a Schmitt-trigger which generates a pulse when the signal is greater than 2 V. The transmitter circuit consists of a MOSFET operated as semiconductor switch, with an additional pull-up resistor connected to +12 V. The measurement starts when the microcontroller generates a square-wave pulse with an adjustable frequency between 20 - 50 kHz. After 50 - 200 μs, depending on the condition of the cell, the microcontroller receives two or more pulses which are generated by the receiver circuit. The microcontroller measures the time between the first falling edge and the second or third rising edge, if any. The first falling edge is the reference pulse which was generated from the microcontroller. This type of setup only requires the use of one general input and output (GPIO) of the microcontroller to generate the pulse for the transmitter circuit, and one enhanced capture module (eCAP) to measure the time elapsed between the triggers generated by the receiving circuit. It has a clock of 100 MHz, leading to a sampling time of 10 ns. This could also be done by combining a fast GPIO or analogue digital converter (ADC) with a timer module if the microcontroller does not have this feature.

The influence on processor load is very low, so the already existing microcontroller of a BMS can be used to perform this task, further driving down the cost of the TOF application. So, in total only some very low-cost components like common operational amplifiers, electronic switches, and passive components are needed to realize the TOF circuit, reducing cost down to the single-digit Euro range, even before considering economies of scale.

The evolution of SOC impacts the overall mechanical impedance of the cell. Thus, not only the TOF shifts, but also the waveform of the signal itself as well. For some cases at the boundary regions of the system, the Schmitt-trigger level could be too low or too high; this generates different trigger sequences. Therefore, the execution of an algorithm that sorts out the pulses and utilizes the correct one is required. The description of the functionality of such an

algorithm is presented as pseudo-code in the supplementary materials.

III. EXPERIMENTAL

This study used commercially available high energy pouch cells from Kokam Company, Ltd. (Gyeonggi-Do, Republic of Korea) type SLPB065070180 [18] with a capacity of 12 Ah and an energy density of 260 Wh/kg (Fig. 1). The cell is composed of a Nickel-Manganese-Cobalt cathode and a graphite anode, representing two commonly used active materials in state-of-the-art Lithium-Ion technology.

Before the actual test the cells were cycled 5 times with a current of 0.5 times the rate of the nominal current (C-rate) between the upper and the lower voltage limit, all according to the manufacturer instructions. Evaluating the TOF approach, under conditions of real-world applications requires tweaking of parameters to which a battery cell's mechanical properties are most sensitive. Despite cycling and storage history, which is negligible in our case of fresh cells, these parameters are temperature [11] and current rates [19]. To estimate the temperature dependency of the TOF approach the arbitrary cell was set at SOC 50 % and subjected to three temperature cycles between 5 and 45°C while the TOF was monitored constantly. Temperature was elevated by 10°C per hour. To estimate the current dependency the cell current on both charge and discharge was set to 0.1, 0.5 and 1 C-rate of the cell under test. Additionally, the cell was discharged with WLTP cycles [13] from SOC 95% until the lower voltage limit was reached. Each cycle lasted 1800 s. The profile was downscaled to cell level and consumed 1.38 Ah of charge, with peak current during the highest discharge pulse set to 18.53 A.

A controlled ambient temperature was secured as all the tests were performed in a calibrated climatic chamber. Temperature was monitored by an in-house developed cell test unit (CTU) via a K-type thermocouple taped onto the upper segment of the cell together with insulation material for decoupling the thermocouple from the ambient temperature. The CTU was also responsible for controlling the cell current and voltage. The channel was calibrated with an accuracy of 0.2 % for the current and 0.1 % for the voltage, both for measured value. Synchronization of the measured TOF by the BMS board (see sec. II) with values obtained by the CTU was done via controller area network (CAN) serial bus protocol; all values were incorporated into the CTU data log file.

All the TOF signals in the following graphs are filtered with a median filter over 100 samples in order to suppress measurement noise.

IV. RESULTS AND DISCUSSION

In Fig. 4 (a) the square wave input signal and the measured and amplified system response of the battery are shown. Both values were measured using an oscilloscope; for normal operation, only the pulses are analysed by the

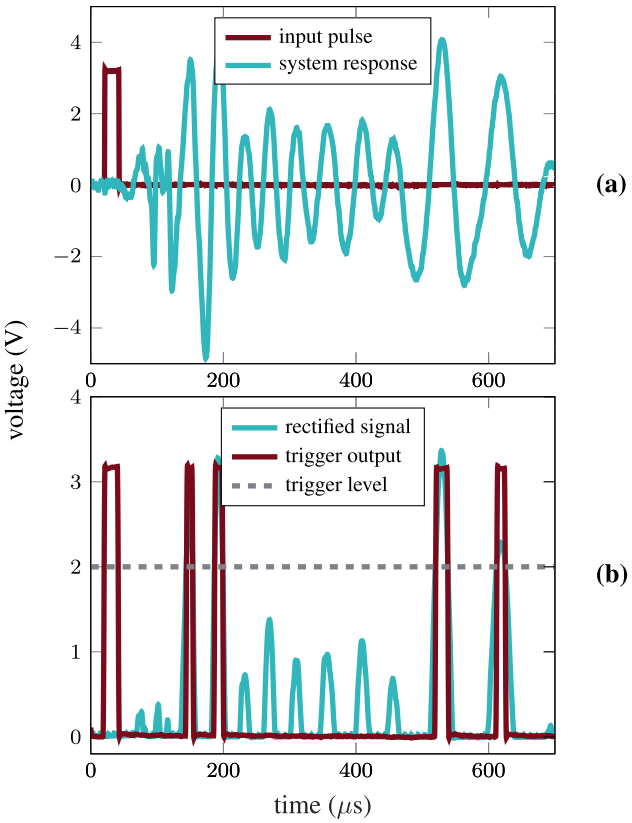

FIGURE 4. Input pulse and system response (a), rectified signal for Schmitt-trigger and trigger output (b).

system. It can be seen that the mechanical excitation via a rectangular pulse leads to a pronounced non-harmonic wave motion of the system with an initial noisy peak after 72 μ s with pronounced half waves starting around 140 μ s, which is in agreement with the values estimated in sec II. To cancel the initial noise, the trigger level needs to be set accordingly.

Fig. 4 (b) depicts the post-processing of the measurement. The amplified signal is rectified by a single diode rectifier so that the subsequent circuitry only needs to process positive signals (see also Fig. 3). The Schmitt-trigger then has a trigger level of 2 V and has a rectangle signal on the output if the value is higher. In the case shown here this is true for two initial pulses and also for the pulses along the signal. The pulses are received on the eCAP input of the microcontroller. This is a capture and counter module. It triggers the first positive edge and then counts the time until the next rising edge is detected. The microcontroller software considers the first two response pulses as relevant and discards the others. Those two pulses are traced and taken for calculation over the entire SOC since the time between the trigger and the edges of the signal represents the TOF and will change over SOC (see also Fig. 3).

The progress of the TOF for a full cycle and different sampling frequencies with a current of 0.5 C-rate is given in Fig. 5, where a correlation of the TOF with

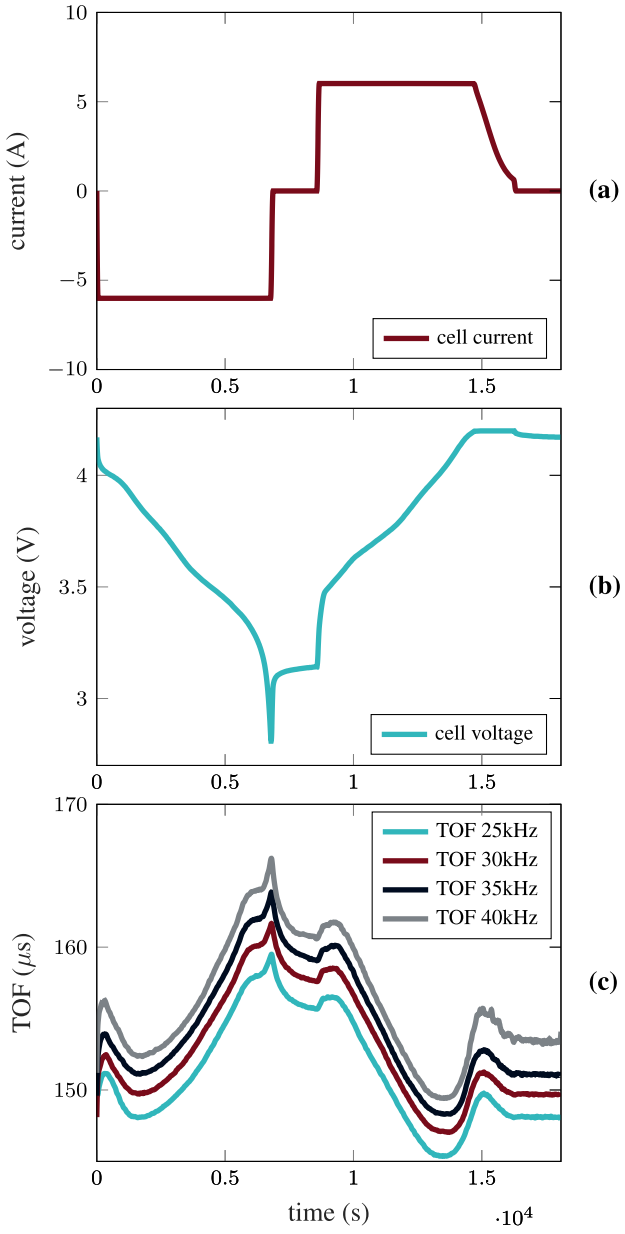

FIGURE 5. Full cycle with voltage (a), current (b) and TOF for several frequencies (c).

the SOC is obvious. As expected (see sec. II), and observed with different approaches in other publications [2], [9], [10], in general the TOF decreases as the SOC increases. Higher frequencies lead to a higher overall TOF, but the progress of the slope over the cycle is similar. Longer TOF also means higher damping of the signal. This is why the TOF at 40 kHz already shows higher distortion in the low SOC region - not all pulses can be detected. However, higher frequencies also could be measured, if necessary, by adapting the parameters of the electronics. The piezo discs chosen for this work have higher attenuation at higher frequencies. Therefore, for the subsequent measurements described in the manuscript a frequency of 30 kHz was chosen.

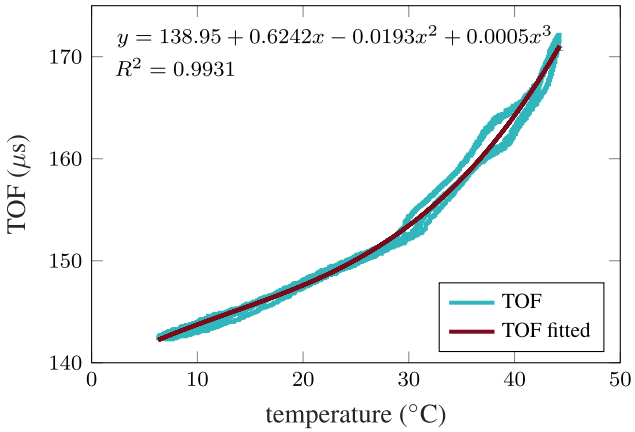

FIGURE 6. Temperature dependency of TOF for the cell at SOC 50 %.

During idle phases the TOF shows a relaxation similar to the one of the cell voltage; thus, after a constant voltage phase during charging the relaxation behaviour is less pronounced compared to the one after constant current discharge. When cell current is applied again, both in the charged and discharged states, the initial peak in TOF is observed again. Bauer *et al.* [20] also observed such behaviour for dilation and attributed it to Lithium staging related phenomena.

Tests on half cells, done separately for anode and cathode of the cells under investigation, have shown that it is most likely local responses resulting from different lithiation stages in the graphite anode [21] that lead to different mechanical properties over the SOC, and thus proves the tendency of an increasing TOF with reducing the SOC. With other cells or other operational parameters also unique TOF to SOC correlations can be observed [2], [12], making the method quite plausible for a BMS application.

In Fig. 6, the dependency of TOF on temperature is depicted. One can see that the TOF declines proportionally to the temperature decrease. This is explained by the higher stiffness of the battery at lower temperatures and thus a higher propagation speed of the wave. The difference between the lowest and the highest TOF is 30 μ s, which is 20 % of the value measured at 25°C. The hysteresis observed in the TOF is related to the temperature level to which the cell was heated or cooled down. This temperature dependency is especially relevant for a real BMS application as batteries in mobile or outdoor stationary applications would endure wide variations in temperature. The slope of the temperature for a BMS can be represented by a 3rd degree polynomial function, also given in Fig. 6. The goodness of the fit is $R^2 = 0.9931$, with a maximum deviation of 2.41 μ s or 1.49 % of measured value at 161.6 μ s. So, a simple compensation of variations in TOF by temperature can be implemented in the BMS when cell temperature is monitored.

Additional uncertainties arise from TOF response as a result of different C-rates. According to Fig. 7, which shows

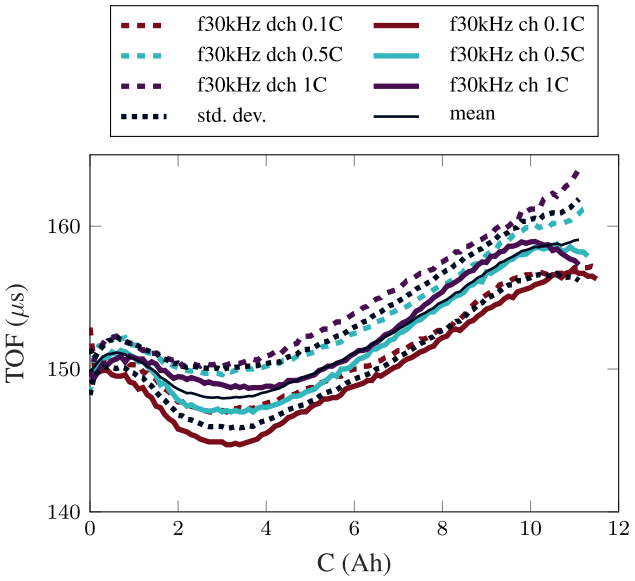

FIGURE 7. TOF for charge and discharge with different C-rates over transferred charge.

the TOF over charge for different profiles with a sample frequency of 30 kHz, higher C-rates lead to longer TOF. Very low C-rates lead to more pronounced local minima at low SOC. Different mechanical behaviour for different C-rates was also observed by Grimsmann *et al.* [19] for dilation. Higher C-rates lead to thinner layers, or indeed thinner cells. The authors attribute this behaviour to inhomogeneous lithium distribution within the electrodes or the particles themselves. This also is believed to influence the TOF as measured here.

Fig. 7 also provides the mean value and the standard deviation calculated for all charge and discharge curves. The highest deviations are observed in higher SOC regions with the maximum of 2.85 μ s from 159.05 μ s at 11.1 Ah, which is an error of 1.79 %. Greater deviations arise from the not clearly determined signal over the SOC. Taking for example the mean value, the peak value of 151.15 μ s at 0.6 Ah can also be found on the curve at 6.1 Ah, which is more than 10 times the SOC value. This means that a BMS with TOF-based state estimation also needs an additional functionality for detection of the position on the curve. Coupling with voltage measurement for a single estimation of a battery in an unknown state or a Kalman filter would be a solution for running operation. A single standalone TOF measurement is not suited for estimation of the SOC in case of the cell under test. This is expected to be different with other types of cells based on the findings regarding TOF progress in other studies [2], [12].

In Fig. 8, the TOF response to consecutive WLTP cycles is shown. To reflect operation in a battery electric vehicle, the cycle starts at a SOC at 95 % and the battery is then exhausted by applying WLTP cycles, each consuming 1.38 Ah. The mean value calculated from the measurements as in Fig. 7 is corrected for the measured cell temperature

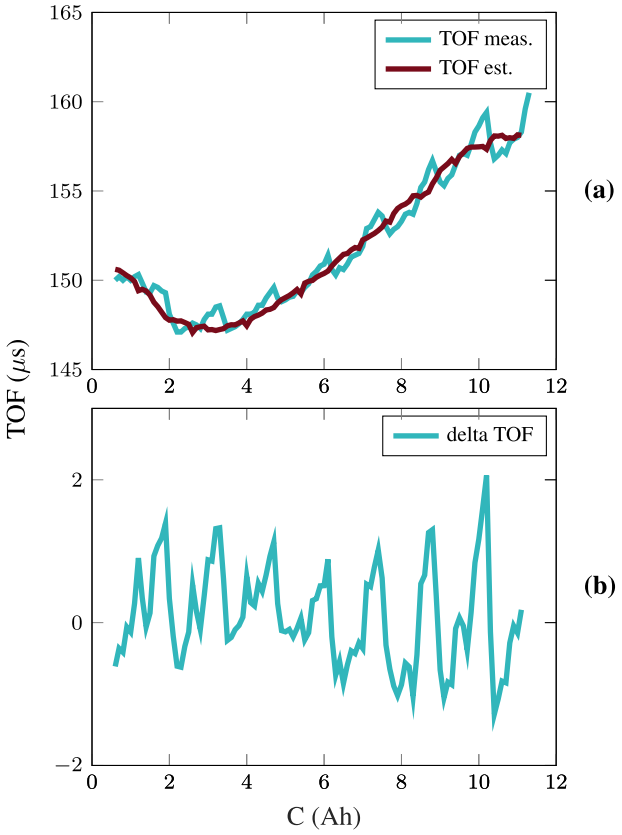

FIGURE 8. TOF measured under driving cycle and estimated TOF (a) and deviation between measured and estimated TOF (b).

during the cycles, with the approach from Fig. 6 serving as an estimator for the TOF to SOC relationship. It can be seen that even during cycles, with such fluctuations between C-rates and charge and discharge, the trend of the TOF is similar to that in constant cycles and the corrected mean value serves as an estimator, producing a maximum error of 2.06 μ s which is an error of 1.29 % of the measured value, or 16.85 % of the total change in TOF, that corresponds to the SOC in the test case. Note that an advanced algorithm like the one described above is necessary to achieve this result.

While the general trend of the SOC over the WLTP is followed by the TOF curve, there are repeating peaks in the real SOC which are not reflected in the TOF curve. These peaks result from the phase with higher power, including peak C-rates of 1.54 C at the end of the WLTP cycle. As shown above, higher C-rates lead to larger changes in the mechanical behaviour of the cell. As the estimator is produced by fitting of mean values, it does not reflect such high peaks. However, after less power intensive sections of the cycle the error is compensated for.

V. CONCLUSION

This work confirmed the correlation between SOC and TOF, using a method that does not require complex laboratory equipment and can be directly implemented into a BMS at

low additional cost. For the first time the approach was validated in real application scenarios for various temperatures, C-rates, and a driving cycle that represents variations in operational parameters comparable to a real application. From the results obtained during this investigation, one should conclude that some variables, like the temperature, have a significant impact on TOF; as there is a change of 30 μs for change in temperature from 5 to 45°C, while for example at 25°C the total variation in TOF between fully charged and discharged cell is 10 μs. Thus, knowledge of the current cell temperature and compensation for it are necessary. While this can be implemented with low effort, the errors caused by non-straightforward dependency of the TOF on the SOC found for the investigated cell, and by the uncertainties stemming from the C-Rate makes the approach less reliable for SOC determination. However, advanced processing of the data, like Kalman filtering or such, would highly improve data usability. Another possible field of application is the surveillance of the mechanical stability of the cell in the pack, which becomes especially interesting after a crash or other mechanical stress.

APPENDIX

As stated above, a LIB consists of multiple different layers. The connection between the layers can be mathematically represented by using the Global Matrix [17], [22], [23].

$$G = \begin{bmatrix} D_{1hb} & D_{2t} & & & & \\ & D_{2b} & D_{3t} & & & \\ & & D_{3b} & \cdots & & \\ & & & \cdots & D_{(n-1)t} & \\ & & & & D_{(n-1)b} & D_{nht} \end{bmatrix} \tag{1}$$

Doing this, each layer again is represented by a Top

$$D_t = \begin{bmatrix} -k & -k \\ -\sqrt{\frac{\omega^2}{c_l^2}-k^2} & \sqrt{\frac{\omega^2}{c_l^2}-k^2} \\ -i\rho(\omega^2-c_s^2k^2) & -i\rho(\omega^2-c_s^2k^2) \\ -i\rho c_s^2 k\sqrt{\frac{\omega^2}{c_l^2}-k^2} & i\rho c_s^2 k\sqrt{\frac{\omega^2}{c_l^2}-k^2} \\ -\sqrt{\frac{\omega^2}{c_s^2}-k^2} & \sqrt{\frac{\omega^2}{c_s^2}-k^2} \\ k & k \\ i\rho c_s^2 k\sqrt{\frac{\omega^2}{c_s^2}-k^2} & -i\rho c_s^2 k\sqrt{\frac{\omega^2}{c_s^2}-k^2} \\ -i\rho(\omega^2-c_s^2k^2) & -i\rho(\omega^2-c_s^2k^2) \end{bmatrix} \tag{2}$$

and a Bottom Matrix,

$$D_b = \begin{bmatrix} ke^{id\sqrt{\frac{\omega^2}{c_l^2}-k^2}} & \frac{k}{e^{id\sqrt{\frac{\omega^2}{c_l^2}-k^2}}} \\ \frac{\sqrt{\frac{\omega^2}{c_l^2}-k^2}}{e^{-id\sqrt{\frac{\omega^2}{c_l^2}-k^2}}} & -\frac{\sqrt{\frac{\omega^2}{c_l^2}-k^2}}{e^{id\sqrt{\frac{\omega^2}{c_l^2}-k^2}}} \\ \frac{i\rho(\omega^2-c_s^2k^2)}{e^{-id\sqrt{\frac{\omega^2}{c_l^2}-k^2}}} & \frac{i\rho(\omega^2-c_s^2k^2)}{e^{id\sqrt{\frac{\omega^2}{c_l^2}-k^2}}} \\ \frac{-2i\rho kc_s\sqrt{\frac{\omega^2}{c_l^2}-k^2}}{e^{-id\sqrt{\frac{\omega^2}{c_l^2}-k^2}}} & -\frac{-2i\rho kc_s\sqrt{\frac{\omega^2}{c_l^2}-k^2}}{e^{id\sqrt{\frac{\omega^2}{c_l^2}-k^2}}} \\ \frac{\sqrt{\frac{\omega^2}{c_s^2}-k^2}}{e^{-id\sqrt{\frac{\omega^2}{c_s^2}-k^2}}} & -\frac{\sqrt{\frac{\omega^2}{c_s^2}-k^2}}{e^{id\sqrt{\frac{\omega^2}{c_s^2}-k^2}}} \\ -ke^{id\sqrt{\frac{\omega^2}{c_s^2}-k^2}} & -\frac{k}{e^{id\sqrt{\frac{\omega^2}{c_s^2}-k^2}}} \\ -\frac{-2i\rho kc_s\sqrt{\frac{\omega^2}{c_s^2}-k^2}}{e^{-id\sqrt{\frac{\omega^2}{c_s^2}-k^2}}} & \frac{-2i\rho kc_s\sqrt{\frac{\omega^2}{c_s^2}-k^2}}{e^{id\sqrt{\frac{\omega^2}{c_s^2}-k^2}}} \\ \frac{i\rho(\omega^2-c_s^2k^2)}{e^{-id\sqrt{\frac{\omega^2}{c_s^2}-k^2}}} & \frac{i\rho(\omega^2-c_s^2k^2)}{e^{id\sqrt{\frac{\omega^2}{c_s^2}-k^2}}} \end{bmatrix} \tag{3}$$

where k is the wave number, ω the angular frequency, c_l the longitudinal wave velocity, c_s the shear wave velocity, ρ the density, and d the thickness of each layer.

To determine the propagation speed of the ultrasonic vibration wave, the determinant of the Global Matrix G has to be found. As G is dependent on the sub-matrices D_t and D_b the factors of these two matrices play a crucial role. The factors c_l and c_s represent the longitudinal and shear velocities of the propagating waves. These velocities are dependent on the Young's modulus. In this context, the wave propagation velocity is dependent on the Young's modulus and therefore connected to the SOC.

To determine the parameters for the calculation above, a cell was dismantled and its physical properties determined by post mortem analysis. For details see [21].

ACKNOWLEDGMENT

The authors want to express their appreciation to Dr. I. Gocheva, Dr. M. Jahn, and Mr. D. Dvorak for the scientific discussions and their comments on earlier versions of the manuscript, and to Mrs. J. Winter and Mr. B. Ganev for correction and polishing of the language.

REFERENCES

[1] M. A. Hannan, M. M. Hoque, A. Hussain, Y. Yusof, and P. J. Ker, "State-of-the-art and energy management system of lithium-ion batteries in electric vehicle applications: Issues and recommendations," *IEEE Access*, vol. 6, pp. 19362–19378, 2018.

[2] L. Gold, T. Bach, W. Virsik, A. Schmitt, J. Mueller, T. E. Staab, and G. Sextl, "Probing lithium-ion batteries' state-of-charge using ultrasonic transmission—Concept and laboratory testing," *J. Power Sources*, vol. 343, pp. 536–544, Mar. 2017. [Online]. Available: http://www.sciencedirect.com/science/article/pii/S0378775317301003

[3] R. Xiong, J. Cao, Q. Yu, H. He, and F. Sun, "Critical review on the battery state of charge estimation methods for electric vehicles," *IEEE Access*, vol. 6, pp. 1832–1843, 2018.

[4] V. A. Sethuraman, L. J. Hardwick, V. Srinivasan, and R. Kostecki, "Surface structural disordering in graphite upon lithium intercalation/deintercalation," *J. Power Sources*, vol. 195, no. 11, pp. 3655–3660, Jun. 2010. [Online]. Available: http://www.sciencedirect.com/science/article/pii/S0378775309022964

[5] D. Schneider, "Silicon anodes will give lithiumion batteries a boost," *IEEE Spectr.*, vol. 56, no. 1, pp. 48–49, Jan. 2019.

[6] J. H. Lee, H. M. Lee, and S. Ahn, "Battery dimensional changes occurring during charge/discharge cycles—Thin rectangular lithium ion and polymer cells," *J. Power Sources*, vols. 119–121, pp. 833–837, Jun. 2003. [Online]. Available: http://www.sciencedirect.com/science/article/pii/S0378775303002817

[7] X. Wang, Y. Sone, and S. Kuwajima, "*In situ* investigation of the volume change in li-ion cell with charging and discharging satellite power applications," *J. Electrochem. Soc.*, vol. 151, no. 2, pp. A273–A280, Jan. 2004. [Online]. Available: http://jes.ecsdl.org/content/151/2/A273.abstract

[8] A. G. Hsieh, S. Bhadra, B. J. Hertzberg, P. J. Gjeltema, A. Goy, J. W. Fleischer, and D. A. Steingart, "Electrochemical-acoustic time of flight: In operando correlation of physical dynamics with battery charge and health," *Energy Environ. Sci.*, vol. 8, pp. 1569–1577, Mar. 2015. [Online]. Available: http://dx.doi.org/10.1039/C5EE00111K

[9] P. Ladpli, F. Kopsaftopoulos, and F.-K. Chang, "Estimating state of charge and health of lithium-ion batteries with guided waves using built-in piezoelectric sensors/actuators," *J. Power Sources*, vol. 384, pp. 342–354, Apr. 2018. [Online]. Available: http://www.sciencedirect.com/science/article/pii/S0378775318301770

[10] P. Ladpli, C. Liu, F. Kopsaftopoulos, and F.-K. Chang, "Estimating lithium-ion battery state of charge and health with ultrasonic guided waves using an efficient matching pursuit technique," in *Proc. IEEE Transp. Electrific. Conf. Expo, Asia–Pacific (ITEC Asia–Pacific)*, Jun. 2018, pp. 1–5.

[11] H. Popp, G. Glanz, K. Alten, I. Gocheva, W. Berghold, and A. Bergmann, "Mechanical frequency response analysis of lithium-ion batteries to disclose operational parameters," *Energies*, vol. 11, no. 3, p. 541, Mar. 2018. [Online]. Available: http://www.mdpi.com/1996-1073/11/3/541

[12] P. Ladpli and F.-K. Chang, "Battery state monitoring using ultrasonic guided waves," U.S. Patent WO 2017 223 219 A1, Jun. 21, 2017.

[13] UNECE - United Nations Economic Commission for Europe. 2017. *WLTP—Worldwide Harmonized Light-Duty Vehicles Test Procedure*. [Online]. Available: www.unece.org/fileadmin/DAM/trans/doc/2012/wp29grpe/WLTP-DHC-12-07e.xls

[14] C. Yang. (2017). *Distributed Piezoelectric Transducers and Their Applications in Structural Health Monitoring*. [Online]. Available: http://dokumentix.ub.uni-siegen.de/opus/volltexte/2017/1101

[15] J. Noël and G. Kerschen, "Nonlinear system identification in structural dynamics: 10 more years of progress," *Mech. Syst. Signal Process.*, vol. 83, pp. 2–35, Jan. 2017. [Online]. Available: http://www.sciencedirect.com/science/article/pii/S088832701630245X

[16] K. R. Kganyago and P. E. Ngoepe, "Structural and electronic properties of lithium intercalated graphite LiC_6," *Phys. Rev. B, Condens. Matter*, vol. 68, Nov. 2003, Art. no. 205111. [Online]. Available: https://link.aps.org/doi/10.1103/PhysRevB.68.205111

[17] R. Lammering, U. Gabbert, M. Sinapius, T. Schuster, and P. E. Wierach, *Lamb-Wave Based Structural Health Monitor. Polymer Composites*. Luxemburg, Germany: Springer, 2018.

[18] *Superior Lithium Polymer Battery (SLPB) Cell Specification*, Kokam Company, Suwon, South Korea, 2017.

[19] F. Grimsmann, F. Brauchle, T. Gerbert, A. Gruhle, M. Knipper, and J. Parisi, "Hysteresis and current dependence of the thickness change of lithium-ion cells with graphite anode," *J. Energy Storage*, vol. 12, pp. 132–137, Aug. 2017. [Online]. Available: http://www.sciencedirect.com/science/article/pii/S2352152X1730097X

[20] M. Bauer, M. Wachtler, and H. Stöwe, J. V. Persson, and M. A. Danzer, "Understanding the dilation and dilation relaxation behavior of graphite-based lithium-ion cells," *J. Power Sources*, vol. 317, pp. 93–102, Jun. 2016. [Online]. Available: http://www.sciencedirect.com/science/article/pii/S0378775316302932

[21] M. Luthfi, "State estimation of lithium ion battery using non-invasive method," M.S. thesis, Carinthia Univ. Appl. Sci., Villach, Austria, 2018.

[22] M. J. S. Lowe, "Matrix techniques for modeling ultrasonic waves in multilayered media," *IEEE Trans. Ultrason., Ferroelectr., Freq. Control*, vol. 42, no. 4, pp. 525–542, Jul. 1995.

[23] A. Demčenko and Mažeika, "Calculation of Lamb waves dispersion curves in multilayered planar structures," *Ultragarsas*, vol. 44, no. 3, pp. 15–17, 2002.

HARTMUT POPP (S'18) received the M.Sc. degree in industrial electronics from FH Technikum Vienna, Austria, and in environment and bioresources management from the BOKU University Vienna, Austria, respectively. He is currently pursuing the Ph.D. degree with the Institute of Electronic Sensor Systems, Technical University Graz, Austria. After working as a Design Engineer at Siemens AG, he joined the AIT Austrian Institute of Technology. His research interests include testing, modelling, and diagnostics of Lithium-Ion batteries. He is a Student Member of IEC/OVE TC21 Working Group.

MARKUS KOLLER received the M.Sc. degree in embedded systems from the University of Applied Science Technikum Vienna, in 2015. Since then, he has been working as a Researcher with the Center for Low-Emission Transport, AIT Austrian Institute of Technology. His field of work includes the development of battery management systems, the software development of active and passive balancing algorithms, and commissioning of battery management systems hardware.

SEVERIN KELLER is currently pursuing the bachelor's degree in mechanical engineering with Hochschule Augsburg. He performed a Practical Semester at the TU Graz Institute of Electronic Sensor Systems. His research interests, concerning his bachelor thesis, include testing and modelling diagnostic systems for Lithium-Ion batteries.

GREGOR GLANZ is currently pursuing the bachelor's degree in mechanical engineering – economics with the Technical University of Vienna. He joined the AIT Austrian Institute of Technology, in 2017, as a Working Student. His field of work and research interests include the mechanical properties and testing of Lithium-Ion batteries.

REINHARD KLAMBAUER received the master's degree in electrical engineering from the University of Technology in Graz, Austria, in 2014. His master thesis was part of the international research project A3 Falcon with the topic spatially resolved impedance spectroscopy in a PEM fuel cell. He worked as a University Project Assistant on various industry projects focusing on embedded systems. Since 2016, he has been employed as a University Assistant with the Institute of Electronic Sensor Systems. He is currently working on his Ph.D. thesis with the preliminary title Ultrasonic in Reactive Flows.

ALEXANDER BERGMANN received the Ph.D. degree in physics from Karl Franzens University, Graz, Austria, in 2000. From 2001 to 2016, he worked in different industrial Research and Development positions in the field of sensors and sensor systems. Since 2016, he has been a Professor and the Head of the Institute of Electronic Sensor Systems, Faculty of Electrical and Information Engineering, Graz University of Technology, Graz. He has coauthored two books, more than 65 articles, and filed more than 20 patents. His main research areas include modelling, simulation and design of electronic sensor systems, aerosol sensors and ambient air sensors, photo- and thermoacoustic sensors, sound, ultrasound and vibration sensors, distributed, multimodel sensors and sensor networks, highly integrated sensors, and sensor systems.